

Observation of a dissipative time crystal

Hans Keßler,¹ Phatthamon Kongkhambut,¹ Christoph Georges,¹
Ludwig Mathey,^{1,2} Jayson G. Cosme,³ and Andreas Hemmerich^{1,2}

¹Zentrum für Optische Quantentechnologien and Institut für Laser-Physik, Universität Hamburg, 22761 Hamburg, Germany

²The Hamburg Center for Ultrafast Imaging, Luruper Chaussee 149, 22761 Hamburg, Germany

³National Institute of Physics, University of the Philippines, Diliman, Quezon City 1101, Philippines

(Dated: March 28, 2022)

The formation of a phase of matter can be associated with the spontaneous breaking of a symmetry. For crystallization, this broken symmetry is the spatial translation symmetry, as the atoms spontaneously localize in a periodic fashion. In analogy to spatial crystals, the spontaneous breaking of temporal translation symmetry results in the formation of time crystals. While recent and on-going experiments on driven isolated systems aim to minimize dissipative processes, as it is an undesired source of decay, well-designed dissipation has been put forth as a constitutive ingredient in the formation of dissipative time crystals (DTCs). Here, we present the first experimental realisation of a DTC, implemented in an atom-cavity system. Its defining feature is a period doubled switching between distinct checkerboard density wave patterns, induced by controlled cavity-dissipation and cavity-mediated interactions. We demonstrate the robustness of this phase against system parameter changes and temporal perturbations of the driving. Our work provides a framework for realising phases of matter with spatiotemporal order in presence of dissipation.

Following its initial proposal^{1,2}, the possibility of time crystals in the ground state of equilibrium many-body systems was ruled out for fundamental reasons^{3,4}. This development led to a paradigm shift in seeking time crystals towards genuine nonequilibrium scenarios^{5–11}. In particular, the no-go theorem^{3,4} can be circumvented by periodic driving, which imposes a discrete time translation symmetry on the system. Floquet or discrete time crystals emerge, when discrete time translation symmetry is spontaneously broken, which manifests as a subharmonic response of an observable^{12–15}. Previous experimental studies have focused on closed quantum systems with long-lived time crystalline response enabled by mechanisms, which impede excessive heating^{5–7,16,17}. The ‘melting’ of a time crystal can also be inhibited by coupling to an environment, which introduces controlled dissipation and fluctuation to the system^{18–23}.

Here, we report the experimental realisation of a dissipative time crystal phase in an atom-cavity platform²⁴. This is inspired by a recent theoretical proposal for a time crystal stabilised through an interplay between interaction and dissipation in the open Dicke model, arising when the light-matter coupling is periodically

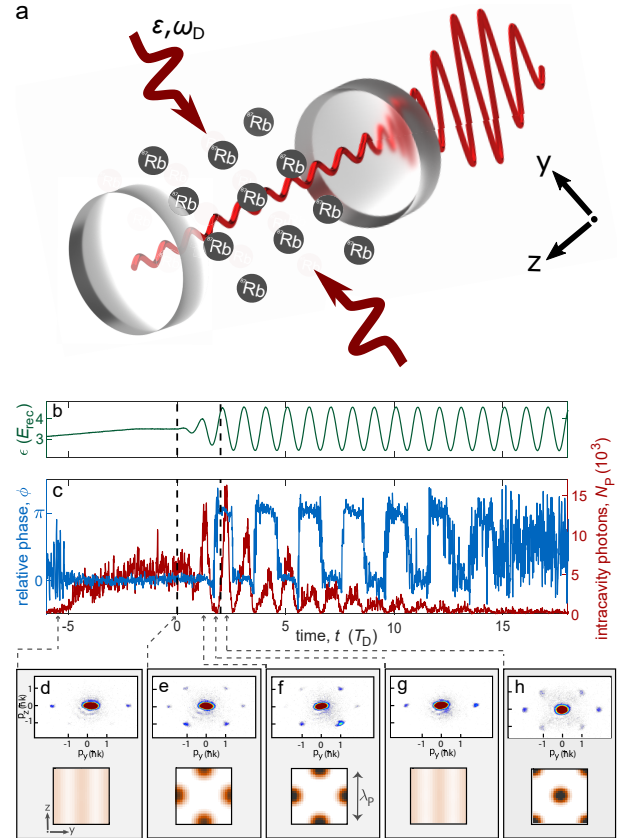


FIG. 1. **Dissipative time crystal.** **a**, Schematic diagram of the transversely pumped atom-cavity system. **b**, Time sequence for the pump with modulation strength $f_0 = 0.3$ and modulation period $T_D = 0.25$ ms. In the time interval delimited by dashed lines, f_0 is linearly ramped from zero to its desired value. **c**, The corresponding response of the intracavity photon number N_P (red) and the relative phase ϕ between the pump and the cavity light field (blue). **d-h**, Top panels: momentum distributions measured at instances of time marked by dashed arrows in **c**. Bottom panels: corresponding mean-field results for the single-particle density distribution, which shows periodic switching between even and odd DWs at twice the driving period.

modulated^{18,19,21}. The defining feature of this paradigmatic DTC is a subharmonic response, where the system periodically switches between pairs of \mathbb{Z}_2 symmetry broken superradiant states.

A Bose-Einstein condensate (BEC) of ^{87}Rb atoms is prepared inside a high-finesse optical cavity pumped by

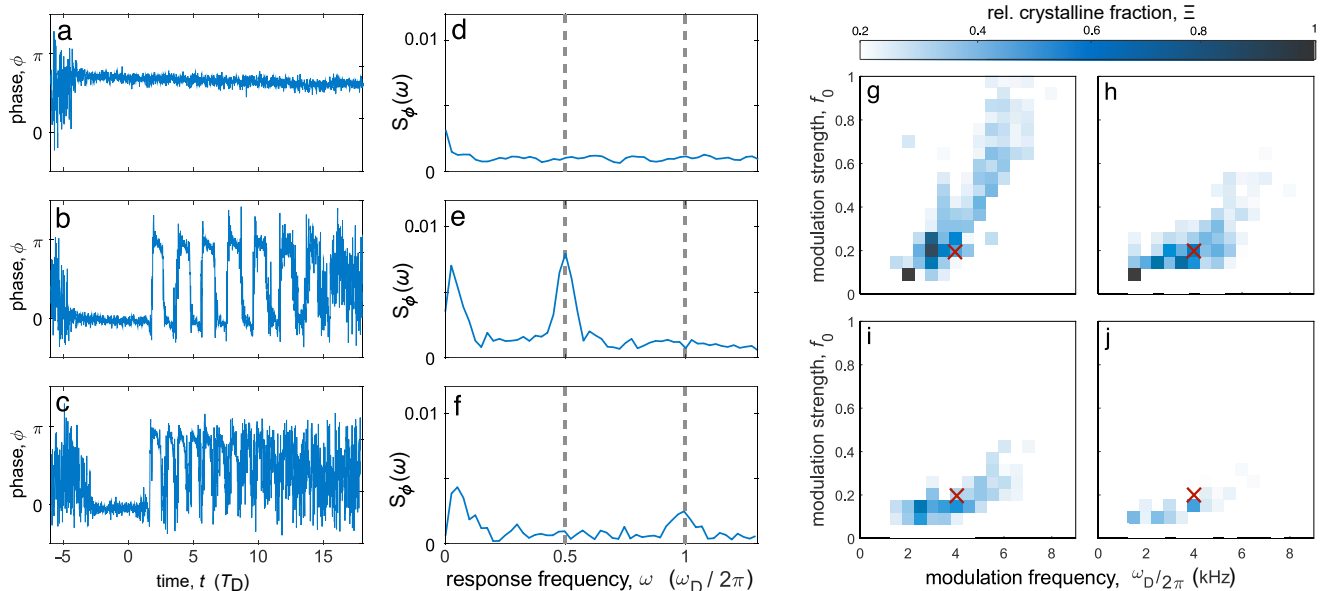


FIG. 2. **Dynamical regimes.** **a-c**, Dynamics of the relative phase ϕ for $f_0 = 0.05$ (**a**), $f_0 = 0.25$ (**b**), and $f_0 = 0.95$ (**c**) with fixed $\omega_D = 2\pi \times 4$ kHz. **d-f**, Corresponding Fourier spectra of the dynamics in **a**, **b**, and **c**. As the modulation strength is increased, the system transforms from a DW to a DTC phase. Strong modulation leads to heating and chaotic behaviour. **g-j**, Dynamical phase diagram showing the relative crystalline fraction Ξ as a function of the modulation frequency ω_D and strength f_0 for clean modulation (**g**), weak noise strength $n = 9.6$ (**h**), intermediate noise strength $n = 15.9$ (**i**), and large noise strength $n = 22.3$ (**j**). The diagram is constructed by dividing the parameter space into 18×18 plaquettes and within each averaging over multiple experimental runs (at least four realizations). Red crosses in **g-j** mark the modulation parameters used in Figs. 3a-d. Increasingly large noise strengths shrink the area in the phase diagram where a stable DTC phase prevails.

a retro-reflected laser beam at wavelength $\lambda_P = 803$ nm, aligned perpendicular to the cavity axis, as depicted in Fig. 1a. The atom-cavity system operates in the recoil-resolved regime, where the cavity field and the atomic distribution evolve at a similar timescale leading to a retarded infinite-range cavity-mediated interaction between the atoms²⁵. Above a critical value of the pump strength ϵ , the system undergoes a self-organisation transition from a BEC phase to a density wave (DW) phase, which emulates the superradiant phase transition in the open Dicke model^{26,27}. In a spontaneous \mathbb{Z}_2 symmetry breaking process, an intracavity optical lattice arises, which traps the atoms either in the black or the white squares of a checkerboard pattern, denoted as odd and even DW.

An effective driving of the light-matter coupling can be realized by modulating the pump strength. Off-resonant driving of the pump strength at a frequency ω_D notably exceeding the recoil frequency $\omega_{\text{rec}} \equiv \hbar k^2 / (2m) = 2\pi \times 3.55$ kHz, with $k \equiv 2\pi / \lambda_P$ and the atomic mass m , leads to a dynamical renormalisation of the phase boundary between the BEC and DW phases^{28,29}. On the other hand, a period doubling response characterised by periodic switching between the odd and even DWs has been predicted for modulation only slightly above the recoil frequency^{18,30,31}. This phase, originally addressed as dynamical normal phase¹⁸, shows subharmonic oscillations between the two \mathbb{Z}_2 symmetry broken even and odd DW

states and is closely related to the DTC phase proposed in the open Dicke model¹⁹. In the following, we describe the experimental realization of this DTC and analyse its properties as a time crystal.

Each experimental sequence begins with preparing the atom-cavity system in the self-organized DW phase (see Methods). An example of a time sequence for the pump is shown in Fig. 1b. For $t < -5T_D$ the system is in the BEC phase. The intracavity photon number N_P is zero and the observed momentum spectrum in the upper panel of Fig. 1d shows the BEC mode at zero momentum and two Bragg resonances at $\pm 2\hbar k$ along the y -direction, associated with the matter grating induced by the pump wave. This grating is illustrated in the lower panel of Fig. 1d by showing the single-particle density distribution obtained from a mean-field model (see Methods). The self-organisation transition into the DW phase is observed in Fig. 1c around $t \approx -5T_D$, as evinced from a significant increase in the intracavity photon number N_P and the locking of the relative phase ϕ between the pump and cavity fields at a constant value $\phi \approx 0$. A momentum spectrum, characteristic for the DW phase, is shown in the upper panel of Fig. 1e for $t = 0$. The occupation of the momentum modes $\{p_y, p_z\} = \{\pm\hbar k, \pm\hbar k\}$ signals the formation of an intracavity checkerboard matter grating, as illustrated by the calculated single-particle density distribution, shown in the lower panel. The two possible energetically degenerate DW states can be dis-

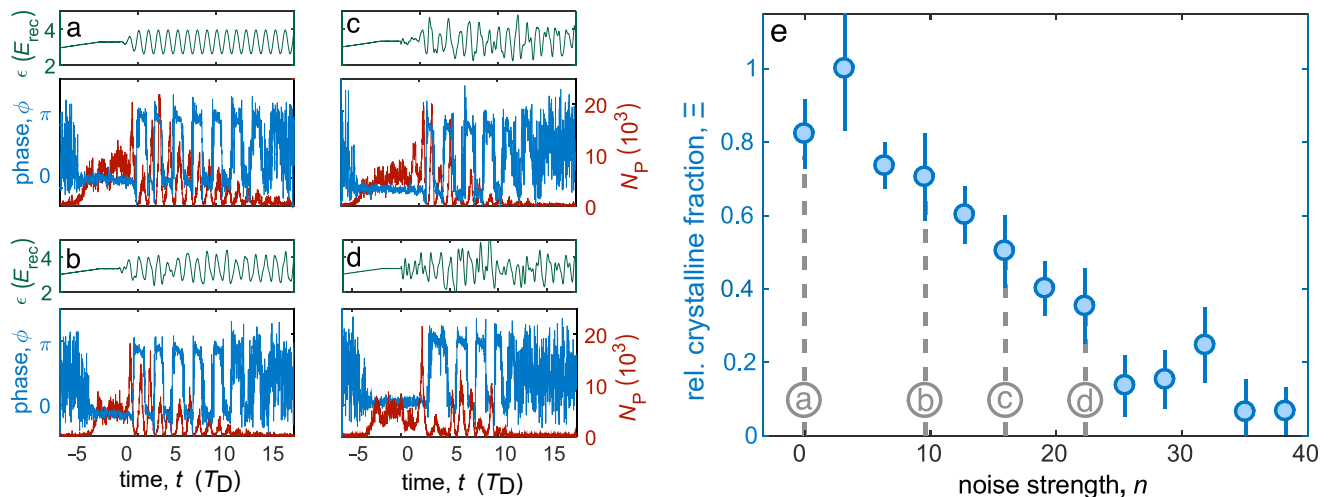


FIG. 3. **Robustness of subharmonic response.** **a-d**, Single-shot experimental runs for the noise strengths applied in Figs. 2g-j and for values of ω_D and f_0 according to the red crosses in these figures. Top panels: single-shot protocols for the pump strength. Bottom panel: corresponding time evolution of the relative phase ϕ (blue trace) and intracavity photon number N_P (red trace). **e**, Dependence of the relative crystalline fraction Ξ on the noise strength averaged over 7 experimental runs with $f_0 = 0.2$ and $\omega_D = 2\pi \times 4$ kHz. The gray dashed lines mark the noise strengths used in **a-d**.

tinguished by their associated values of the phase $\phi = 0$ or $\phi = \pi$ for odd and even realizations, respectively³². We measure N_P and ϕ using a balanced heterodyne detection scheme³³. The probability for the occurrence of the odd and even DW configurations is found to be close to 50% (see Methods), which confirms that the discrete symmetry breaking in the checkerboard DW phase is well established in our system.

Upon preparation of the DW phase, in the time interval delimited by the vertical dashed lines, we linearly increase the modulation strength f_0 in $500 \mu\text{s}$ from zero to its final value (see Fig. 1b). Subsequently, f_0 is kept constant for 5 ms, such that the pump strength evolves according to $\epsilon = \epsilon_0[1 + f_0 \sin(\omega_D t)]$. The dynamical response seen in Fig. 1c for positive t , presents the key observation of this work: the emergence of a DTC phase characterised by pulsating behaviour of the intracavity photon number N_P (red trace) and a period-doubling response of the relative phase ϕ (blue trace). The presence of intracavity photons highlights the many-body aspect of the DTC phase since they induce a retarded infinite-range interaction or all-to-all coupling between the atoms. The period-doubling dynamics arises in the relative phase ϕ . As ϕ switches from zero to π or vice-versa after one modulation cycle, the atomic ensemble self-organises from one type of checkerboard lattice (see Fig. 1f) to its symmetry-broken partner (see Fig. 1h). That is, the system requires two modulation cycles to return to its initial configuration. After half of a modulation period, the system crosses from the DW phase with significant occupation of the cavity mode, to the BEC phase, where the cavity is almost empty. This behaviour, corroborated by the momentum distribution in Fig. 1g, is responsible for the pulsating intracavity photon number in Fig. 1c (red trace).

In Fig. 2a-f, we present the various dynamical regimes accessed by tuning the modulation strength. For weak modulation (see Figs. 2a and 2d), the system stays in the DW phase and the relative phase remains locked to its value before the pump modulation. For intermediate modulation strength, the relative phase exhibits period-doubling dynamics (see Fig. 2b), resulting in a subharmonic peak at $\omega = \omega_D/2$ in the Fourier spectrum in Fig. 2e. Increasing the modulation strength even further leads to chaotic dynamics dominated by heating and loss of spatiotemporal coherence (see Figs. 2c and 2f). In contrast to the coherent switching observed in the DTC phase, the chaotic phase is characterised by intermittent dynamics of the relative phase, whereby the system appears to get stuck in one type of checkerboard pattern for two or more consecutive driving cycles (see Fig. 2c).

Next, we test the robustness of the DTC against variations of the system parameters and temporal perturbations. To this end, we calculate the relative crystalline fraction Ξ ^{6,7}, defined by means of the amplitude of the subharmonic peak in the normalised Fourier spectrum $S_\phi(\omega)$ of the relative phase ϕ rescaled by its maximum, i.e., $\Xi = S_\phi(\omega_D/2)/S_{\max,\phi}$, where $S_{\max,\phi}$ is the maximum crystalline fraction measured in the parameter space spanned by $f_0 \in [0, 1]$ and $\omega_D \in 2\pi \times [0, 9]$ kHz. Figure 2g displays the relative crystalline fraction for varying modulation parameters ω_D and f_0 . We observe large relative crystalline fractions $\Xi > 0.2$ for modulation frequencies $\omega_D \in 2\pi \times [2, 8]$ kHz signalling a robust DTC order for a wide range of modulation parameters. Note that the overall shape of the relative crystalline fraction in Fig. 2g resembles the stability island of the DTC obtained from numerical simulations using a simple mean-field model (see Methods and Fig. 6).

To explore the robustness of the DTC against tem-

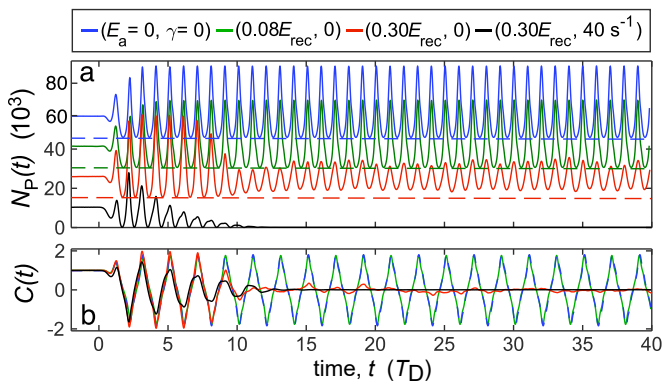


FIG. 4. **Short-range interaction and atom loss.** Numerical results from TWA for the dynamics of the intracavity photon number N_P (a) and the non-equal time correlation C of the photons (b) for different values of the collisional interaction energy E_a and the atom loss rate γ . To increase the quality of the presentation, the black, red, green, and blue traces in a are plotted with different offsets 0, 15, 30, 45×10^3 , respectively. The modulation parameters are $\omega_D = 2\pi \times 4$ kHz and $f_0 = 0.2$.

poral perturbations, we introduce a disorder in time by superimposing Gaussian white noise onto the signal of the pump strength. The noise strength is measured by $n \equiv \sum_{\omega=0}^{2\pi \times 50 \text{ kHz}} |\mathcal{E}_{\text{noisy}}(\omega)| / \sum_{\omega=0}^{2\pi \times 50 \text{ kHz}} |\mathcal{E}_{\text{clean}}(\omega)|$, where $\mathcal{E}_{\text{noisy}}$ ($\mathcal{E}_{\text{clean}}$) is the Fourier spectrum of the pump in the presence (absence) of white noise. Figures 2h-j show how the relative crystalline fraction changes with increasing noise strength. The area with clear DTC response, i.e., a large relative crystalline fraction, shrinks as the noise strength increases. Nevertheless, we still find a sizeable region, where a DTC phase exists, for relatively large noise strength (Fig. 2j). For a fixed set of modulation parameters marked by the red crosses in Figs. 2g-j, typical single-shot results for varying noise strengths are depicted in Figs. 3a-d. Note that even for a strongly distorted pump signal, as in Figs. 3c and 3d, the system still switches multiple times between the two sublattices before the intracavity photons disappear. The relative crystalline fraction at fixed modulation parameters decreases with increasing noise strength, as shown in Fig. 3e. The small offset for large noise strength $n > 25$ is due to the background noise in the Fourier spectrum (see Fig. 2f). Our experimental findings suggest that the DTC in the modulated atom-cavity system is robust against fluctuations not only from the non-unitary dynamics of the dissipative cavity but also from temporal disorder added via driving.

Finally, we address the decay of the time-translation symmetry breaking response in the DTC phase, for example, seen in Fig. 3a. The experimental lifetimes of time crystal implementations are generally finite due to a combination of technical limitations and undesired relaxation dynamics^{5-7,16,17}. In our experiment, the main cause for the decay of time-crystal dynamics can be attributed to

two factors: (i) short-range collisional interaction and (ii) atom losses. In the case of the open Dicke model, the all-to-all coupling between the atoms makes it amenable to a mean-field description. In this theoretical limit, the mean-field solvability of the Dicke model provides the Dicke DTC with the necessary long-range spatiotemporal order and robustness such that it can persist to infinitely long times^{19,21}. However, when mean-field breaking terms are present, the DTC may become unstable, leading to a decay of the symmetry breaking response²¹. In the atom-cavity system, the short-range interaction between the atoms competes with the collective coupling, induced by the cavity photons, and breaks the mean-field solvability of the model. To investigate the damping effects of short-range interaction and atom loss, we employ the truncated Wigner approximation (TWA). The transversely pumped atom-cavity system is thereby modelled by considering only the degrees of freedom along the pump (y direction) and the cavity (z direction) axes (see Methods). The short-range interaction is quantified in terms of the mean-field collisional interaction energy $E_a = (U_a/N_a) \int dydz |\psi_0(y,z)|^4$, where U_a denotes the effective two-dimensional interaction strength (see Methods), N_a is the number of atoms and $\psi_0(y,z)$ is the wave function of the homogeneous BEC. We also include in our model a phenomenological atom loss channel described by $dN_a/dt = -2\gamma N_a$. We simulate the dynamics of the intracavity photon number $N_P = \langle \hat{a}^\dagger \hat{a} \rangle$, where \hat{a} (\hat{a}^\dagger) is the bosonic operator that annihilates (creates) a photon in the single-mode cavity. To characterise temporal long-range order, we calculate the two-point temporal correlation function $C(t) = \text{Re}[\langle \hat{a}^\dagger(t) \hat{a}(t_0) \rangle] / \langle \hat{a}^\dagger(t_0) \hat{a}(t_0) \rangle$ at $t_0 = 0$, the time before the modulation is switched on.

The resulting evolution of $N_P(t)$ and $C(t)$ is studied in Fig. 4 for different values of E_a . First, we consider the dynamics in the absence of atom loss. For weak interaction strength $E_a = 0.08E_{\text{rec}}$, $N_P(t)$ and $C(t)$ in the green traces of Fig. 4 are practically indistinguishable from the findings for $E_a = 0$ in the blue traces. However, stronger short-range interactions with $E_a = 0.30E_{\text{rec}}$ lead to a metastable DTC, where the period-doubling oscillations in $C(t)$ decay after a few cycles, as seen in the red trace in Fig. 4b. This translates to irregular dynamics of the corresponding intracavity photon number $N_P(t)$ (red trace in Fig. 4a) in the long-time regime. Introducing an atom loss channel with $\gamma = 40 \text{ s}^{-1}$, which models the observed atom decay rate in the experiment, yields exponentially decaying behaviour as shown in the black traces in Fig. 4. This behaviour closely resembles the characteristic exponential decay of N_P in our experiment, such that the cavity is almost empty for $t/T_D > 15$ (see Fig. 3a-d). Atom loss leads to a trivial suppression of the atom-cavity coupling and hence of intracavity photons. When the number of intracavity photons falls below the detection level, the relative phase ϕ becomes ill-defined leading to the fast and irregular oscillations of ϕ seen in Fig. 3a-d for late times.

Our observations confirm the realization of a dissipa-

tive time crystal in an atom-cavity system with defining feature of period-doubling dynamics. This quintessential DTC is robust against changes of the system parameters and temporal perturbations added to the drive, thereby fulfilling the robustness property of time crystals. Numerical results based on a simplified semiclassical model imply that short-range interaction and atom loss limits the lifetime of the DTC phase. Beyond proving the existence of dissipative time crystals, our work enables a methodology to understand the foundational properties and potential applications of time crystals in platforms with dissipation, which is ubiquitous in nature. More generally, our work points out how to design non-equilibrium order and functionalities in hybrid quantum matter, beyond the standard notions of equilibrium order, via light control.

ACKNOWLEDGMENTS

This work is funded by the Deutsche Forschungsgemeinschaft (DFG, German Research Foundation) – SFB-925 – project 170620586 and the Cluster of Excellence “Advanced Imaging of Matter” (EXC 2056), Project No. 390715994.

METHODS

Experimental details. The experimental set-up, as sketched in Fig. 1a, is comprised of a magnetically trapped BEC of $N_a = 65 \times 10^3$ ^{87}Rb atoms, dispersively coupled to a narrow-band high-finesse optical cavity. The cavity field has a decay rate of $\kappa = 2\pi \times 4.55$ kHz, which is the same order of magnitude as the recoil frequency $\omega_{\text{rec}} = E_{\text{rec}}/\hbar = 2\pi \times 3.55$ kHz. The wavelength of the pump laser is $\lambda_P = 803$ nm, which is red detuned with respect to the relevant atomic transition of ^{87}Rb at 795 nm. The maximum light shift per atom is $U_0 = -2\pi \times 0.36$ Hz. We fix the effective detuning to $\delta_{\text{eff}} \equiv \delta_C - (1/2)N_a U_0 = -2\pi \times 18.5$ kHz, where $\delta_C = \omega_P - \omega_C$ is the pump-cavity detuning. An experimental sequence starts by preparing the system in the self-organized DW phase. This is achieved by linearly increasing the pump strength ϵ from zero to its final value $\epsilon_0 = 3.3 E_{\text{rec}}$ in 10 ms at a fixed cavity pump detuning $\delta_{\text{eff}} = -2\pi \times 18.5$ kHz.

\mathbb{Z}_2 symmetry breaking. Due to optical path length drifts, we cannot compare the phase ϕ for DW realisations of different experimental runs. The stability of our balanced heterodyne detection is however sufficient to compare the phase for two subsequent DW realisations within the same experimental sequence applying the pump protocol in Fig. 5a. In a perfect system, the phase difference $\delta\phi$ between two subsequent realizations of the DW phase can take two values $\delta\phi = 0$ or $\delta\phi = \pi$ and does not depend on any system

parameters. Since the underlying discrete symmetry breaks spontaneously, we expect equiprobable realisation of the two possible outcomes shown in Figs. 5b and c. The relative occurrence of $\delta\phi$ for 397 realisations is plotted in Fig. 5d using a binning of 0.08π . The two maxima, corresponding to $\delta\phi = 0$ and $\delta\phi = \pi$, are clearly distinguishable and the ratio of all realisations where $\delta\phi \in [-\frac{\pi}{2}, \frac{\pi}{2}]$ over $\delta\phi \in [\frac{\pi}{2}, \frac{3}{2}\pi]$ is 1.15. This number is close to unity, which shows that the \mathbb{Z}_2 symmetry in our system is well established.

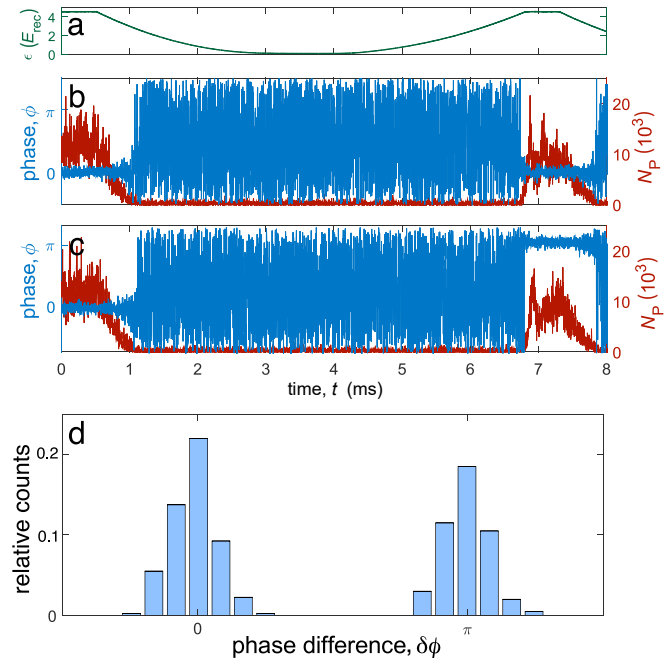


FIG. 5. \mathbb{Z}_2 symmetry breaking. **a** Pump protocol starting in the DW phase, tuning into the BEC phase and back to the DW phase. **b,c** Relative phases ϕ (blue) and intracavity photon numbers N_P (red) measured by heterodyne detector for single experimental runs showing the two typical outcomes $\delta\phi \approx 0$ (b) and $\delta\phi \approx \pi$ (c). **d** Histogram of the phase difference $\delta\phi$ for 397 experimental runs.

Theoretical model. In the frame rotating at the pump frequency $\omega_P = 2\pi/\lambda_P$, the Hamiltonian for the system reads^{24,34}

$$\hat{H} = \hat{H}_C + \hat{H}_A + \hat{H}_{AA} + \hat{H}_{AC}. \quad (1)$$

In Eq. (1), the Hamiltonian for the cavity with a single mode function $\cos(kz)$ is

$$\hat{H}_C = -\hbar\delta_C \hat{a}^\dagger \hat{a}, \quad (2)$$

where \hat{a} (\hat{a}^\dagger) is the cavity mode annihilation (creation) operator. The single-particle Hamiltonian for the atoms is given by

$$\hat{H}_A = \int dy dz \hat{\Psi}^\dagger(y, z) \left[-\frac{\hbar^2}{2m} \nabla^2 + \epsilon \cos^2(ky) \right] \hat{\Psi}(y, z), \quad (3)$$

where m is the mass of an atom and $\hat{\Psi}(y, z)$ is the atomic field operator. The short-range collisional interaction between the atoms is captured by the Hamiltonian

$$\hat{H}_{AA} = U_a \int dydz \hat{\Psi}^\dagger(y, z) \hat{\Psi}^\dagger(y, z) \hat{\Psi}(y, z) \hat{\Psi}(y, z). \quad (4)$$

The effective 2D interaction strength is $U_a = \sqrt{2\pi} a_s \hbar^2 / m \ell_x$, where a_s is the s -wave scattering length and ℓ_x is the harmonic oscillator length in the x direction. The Hamiltonian for the light-matter interaction reads

$$\begin{aligned} \hat{H}_{AC} = \hbar U_0 \int dydz \hat{\Psi}^\dagger(y, z) & \left[\cos^2(kz) a^\dagger a \right. \\ & \left. + \alpha_P (a + a^\dagger) \cos(ky) \cos(kz) \right] \hat{\Psi}(y, z), \end{aligned} \quad (5)$$

where $\alpha_P \equiv \sqrt{\epsilon/\hbar|U_0|}$ is the unitless amplitude of the pump field. The dynamics of the system follows from the Heisenberg-Langevin equations,

$$\frac{\partial}{\partial t} \hat{\Psi} = \frac{i}{\hbar} [\hat{H}, \hat{\Psi}] \quad (6)$$

$$\frac{\partial}{\partial t} \hat{a} = \frac{i}{\hbar} [\hat{H}, \hat{a}] - \kappa \hat{a} + \xi, \quad (7)$$

where the stochastic noise term ξ satisfies $\langle \xi^*(t) \xi(t') \rangle = \kappa \delta(t - t')$. We simulate the dynamics in the semiclassical limit by transforming $\hat{\Psi}$ and \hat{a} into classical fields according to the TWA method³⁵⁻³⁷.

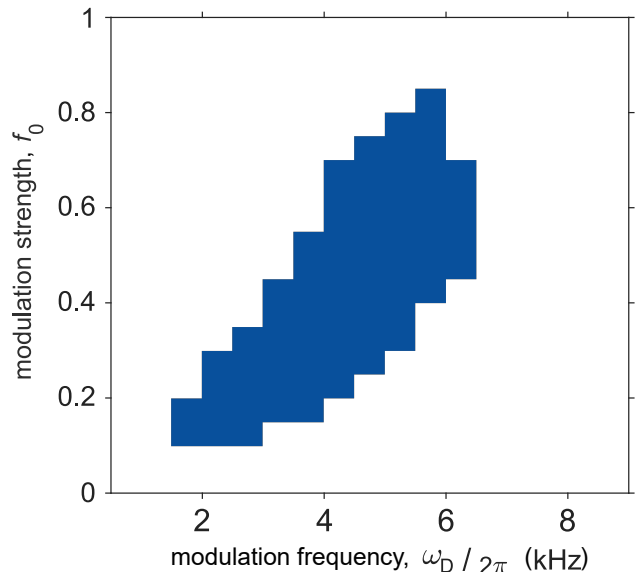


FIG. 6. **Mean-field stability region of the DTC.** Blue area denotes the region in the (f_0, ω_D) -plane where a stable period-doubling response exists within the mean-field model in the absence of short-range interaction.

The TWA is a semiclassical phase space method that goes beyond mean-field theory and can be utilised to test the robustness of time crystals against quantum and stochastic noise due to the dissipative cavity^{31,38}. We numerically integrate the resulting equations of motion for an ensemble of 10^3 initial conditions, which sample the initial quantum noise in the fields and the stochastic noise due to the dissipative cavity. In our simulations, apart from ϵ_0 chosen as $\epsilon_0 = 1.03 \epsilon_{cr}$, where ϵ_{cr} is the critical pump strength for the BEC-DW phase transition, we use the same parameters and protocol for the pump strength as in the experiment. In the comparison of calculations of $N_P(t)$ and $C(t)$ for variable collisional interaction strengths E_a in Fig. 4, we adjust the pump strengths such that the number of intracavity photons in the DW phase is fixed to the same value.

Mean-field phase diagram. In order to obtain a rough orientation with regard to the system parameters suitable for the appearance of a DTC phase, we construct a dynamical phase diagram in the clean mean-field limit, wherein the mean-field breaking short-range interaction is neglected. In particular, we seek period-doubling solutions, which are stable for at least 40 modulation cycles. As depicted in Fig. 6, modulation frequencies in the range $\omega_D \in 2\pi \times [2, 8]$ kHz provide an island with a stable DTC phase. This is consistent with the experimental results in Fig. 2g.

¹ Wilczek, F. Quantum Time Crystals. *Phys. Rev. Lett.* **109**, 160401 (2012).

² Shapere, A. & Wilczek, F. Classical time crystals. *Phys.*

- Rev. Lett.* **109**, 160402 (2012).
- ³ Bruno, P. Impossibility of spontaneously rotating time crystals: A no-go theorem. *Phys. Rev. Lett.* **111**, 070402 (2013).
 - ⁴ Watanabe, H. & Oshikawa, M. Absence of quantum time crystals. *Phys. Rev. Lett.* **114**, 251603 (2015).
 - ⁵ Zhang, J. *et al.* Observation of a discrete time crystal. *Nature* **543**, 217–220 (2017).
 - ⁶ Choi, S. *et al.* Observation of discrete time-crystalline order in a disordered dipolar many-body system. *Nature* **543**, 221–225 (2017).
 - ⁷ Rovny, J., Blum, R. L. & Barrett, S. E. Observation of Discrete-Time-Crystal Signatures in an Ordered Dipolar Many-Body System. *Phys. Rev. Lett.* **120**, 180603 (2018).
 - ⁸ Sacha, K. & Zakrzewski, J. Time crystals: a review. *Rep. Prog. Phys.* **81**, 016401 (2018).
 - ⁹ Else, D. V., Monroe, C., Nayak, C. & Yao, N. Y. Discrete time crystals. *Annu. Rev. Condens. Matter Phys.* **11**, 467–499 (2020).
 - ¹⁰ O’Sullivan, J. *et al.* Signatures of discrete time crystalline order in dissipative spin ensembles. *New Journal of Physics* **22** (2020).
 - ¹¹ Lazarides, A., Roy, S., Piazza, F. & Moessner, R. Time crystallinity in dissipative Floquet systems. *Physical Research* **2**, 1–6 (2020). 1904.04820.
 - ¹² Sacha, K. Modeling spontaneous breaking of time-translation symmetry. *Phys. Rev. A* **91**, 033617 (2015).
 - ¹³ Else, D. V., Bauer, B. & Nayak, C. Floquet Time Crystals. *Phys. Rev. Lett.* **117**, 090402 (2016).
 - ¹⁴ Yao, N. Y., Potter, A. C., Potirniche, I.-D. & Vishwanath, A. Discrete Time Crystals: Rigidity, Criticality, and Realizations. *Phys. Rev. Lett.* **118**, 030401 (2017).
 - ¹⁵ Khemani, V., Lazarides, A., Moessner, R. & Sondhi, S. L. Phase Structure of Driven Quantum Systems. *Physical Review Letters* **116**, 250401 (2016). 1508.03344.
 - ¹⁶ Autti, S., Eltsov, V. B. & Volovik, G. E. Observation of a Time Quasicrystal and Its Transition to a Superfluid Time Crystal. *Phys. Rev. Lett.* **120**, 215301 (2018).
 - ¹⁷ Smits, J., Liao, L., Stoof, H. T. & Van Der Straten, P. Observation of a Space-Time Crystal in a Superfluid Quantum Gas. *Phys. Rev. Lett.* **121**, 185301 (2018).
 - ¹⁸ Chitra, R. & Zilberberg, O. Dynamical many-body phases of the parametrically driven, dissipative Dicke model. *Phys. Rev. A* **92**, 1–7 (2015).
 - ¹⁹ Gong, Z., Hamazaki, R. & Ueda, M. Discrete Time-Crystalline Order in Cavity and Circuit QED Systems. *Phys. Rev. Lett.* **120**, 40404 (2018).
 - ²⁰ Buča, B., Tindall, J. & Jaksch, D. Non-stationary coherent quantum many-body dynamics through dissipation. *Nat. Commun.* **10**, 1730 (2019).
 - ²¹ Zhu, B., Marino, J., Yao, N. Y., Lukin, M. D. & Demler, E. A. Dicke time crystals in driven-dissipative quantum many-body systems. *New J. Phys.* **21**, 073028 (2019).
 - ²² Yao, N. Y., Nayak, C., Balents, L. & Zaletel, M. P. Classical discrete time crystals. *Nat. Phys.* **16**, 438–447 (2020).
 - ²³ Taheri, H., Matsko, A. B., Maleki, L. & Sacha, K. All-Optical Dissipative Discrete Time Crystals. *arXiv: 2012.07927* (2020).
 - ²⁴ Ritsch, H., Domokos, P., Brennecke, F. & Esslinger, T. Cold atoms in cavity-generated dynamical optical potentials. *Rev. Mod. Phys.* **85**, 553–601 (2013).
 - ²⁵ Klinder, J., Keßler, H., Georges, C., Vargas, J. & Hemmerich, A. Bose-einstein condensates in an optical cavity with sub-recoil bandwidth. *Appl. Phys. B* **122**, 765–789 (2016).
 - ²⁶ Baumann, K., Guerlin, C., Brennecke, F. & Esslinger, T. Dicke quantum phase transition with a superfluid gas in an optical cavity. *Nature* **464**, 1301–1306 (2010).
 - ²⁷ Klinder, J., Keßler, H., Wolke, M., Mathey, L. & Hemmerich, A. Dynamical phase transition in the open Dicke model. *Proc. Natl. Acad. Sci. USA* **112**, 3290–3295 (2015).
 - ²⁸ Cosme, J. G., Georges, C., Hemmerich, A. & Mathey, L. Dynamical Control of Order in a Cavity-BEC System. *Phys. Rev. Lett.* **121**, 153001 (2018).
 - ²⁹ Georges, C., Cosme, J. G., Mathey, L. & Hemmerich, A. Light-Induced Coherence in an Atom-Cavity System. *Phys. Rev. Lett.* **121**, 220405 (2018).
 - ³⁰ Molognini, P., Papariello, L., Lode, A. U. & Chitra, R. Superlattice switching from parametric instabilities in a driven-dissipative Bose-Einstein condensate in a cavity. *Phys. Rev. A* **98**, 1–9 (2018).
 - ³¹ Cosme, J. G., Skulte, J. & Mathey, L. Time crystals in a shaken atom-cavity system. *Phys. Rev. A* **100**, 053615 (2019).
 - ³² Baumann, K., Mottl, R., Brennecke, F. & Esslinger, T. Exploring Symmetry Breaking at the Dicke Quantum Phase Transition. *Phys. Rev. Lett.* **107**, 140402 (2011).
 - ³³ Pino, J. M., Wild, R. J., Makotyn, P., Jin, D. S. & Cornell, E. A. Photon counting for Bragg spectroscopy of quantum gases. *Phys. Rev. A* **83**, 1–6 (2011).
 - ³⁴ Nagy, D., Szirmai, G. & Domokos, P. Self-organization of a Bose-Einstein condensate in an optical cavity. *Eur. Phys. J. D* **48**, 127–137 (2008).
 - ³⁵ Polkovnikov, A. Phase space representation of quantum dynamics. *Ann. Phys.* **325**, 1790 (2010).
 - ³⁶ Blakie, P. B., Bradley, A. S., Davis, M. J., Ballagh, R. J. & Gardiner, C. W. Dynamics and statistical mechanics of ultra-cold Bose gases using c-field techniques. *Adv. Phys.* **57**, 363–455 (2008).
 - ³⁷ Carusotto, I. & Ciuti, C. Quantum fluids of light. *Rev. Mod. Phys.* **85**, 299–366 (2013).
 - ³⁸ Keßler, H., Cosme, J. G., Georges, C., Mathey, L. & Hemmerich, A. From a continuous to a discrete time crystal in a dissipative atom-cavity system. *New J. Phys.* **22**, 085002 (2020).